The University of Arizona

Aberration Control in Antique Telescope Objectives

A Master's Report by
Samuel R. Driscoll

In partial fulfillment for the degree of Master of Science
in the
College of Optical Sciences

May 2015

The University of Arizona

ABSTRACT

College of Optical Sciences

Master of Science

by Samuel Driscoll

The development and implementation of achromatic objective lenses in refracting telescopes had a significant impact on image quality and understanding of aberrations in the 18th and 19th centuries. It is common for non-rotationally symmetric errors to be polished into the surfaces of the elements of a telescope objective during the optical manufacturing process. Astigmatism is the most common type of manufacturing error, resulting in a reduction of image quality. Certain achromatic doublets and triplets from the early-mid 1800s have been found to be "clocked" to restrict elements from rotating when mounted in their cells. This paper summarizes different tests performed on these refracting telescope objectives to determine the reasoning behind clocking these lenses and to show how astigmatism was controlled in these telescope objectives.

ACKNOWLEDGEMENTS

I would like to personally thank many of those who greatly supported and guided me through the completion of this report. Most notably is my advisor, Dr. John Greivenkamp who gave me the inspiration and motivation necessary to succeed in my journey. In addition to Dr. Greivenkamp, I would like to recognize David Steed and the Museum of Optics for their help in procuring and identifying the unique telescope objective, which are the focus of this report. I also would like to acknowledge the other members of my review committee, Dr. Sasian and Dr. Schwiegerling for their time and insight. Thank you all very much.

I also wish to express my gratitude to my family, friends, and colleagues. All of whom are responsible for helping me make it to this point in my life. In particular, I further wish to recognize Jason Micali for all of his assistance in the completion of this project and report.

Table of Contents

List of Figures

List of Tables

Chapter 1

Introduction

This report focuses on trying to better understand why certain antique refracting telescope objectives were engineered and manufactured in a particular manner. The objectives of interest were made by the Dollond company in the early to mid-1800's and have particular features associated with them. The lens elements and corresponding cells have been "clocked" to restrict rotational movement once mounted inside the cell. "Clocked' is defined as grinding notches into the edges of the lenses and placing a raised groove in the mounting cell, which serves as a male mate to the female notches. Several of these types of telescope objectives have been found in the collection of the Museum of Optics at the University of Arizona. A hypothesis as to why these lenses were clocked was proposed by Greivenkamp and Steed in their article *The History of Telescopes and Binoculars: An Engineering Perspective* [1]. They state that it was done to minimize the effects of surface astigmatism, as it is a common optical manufacturing error to polish non-rotationally symmetric errors into the individual surfaces of the lens elements that make up a telescope objective. This report will discuss the evolution of the refracting telescope, reasoning behind the astigmatism hypothesis, and tests performed to determine the purpose of clocking these objective lenses.

1.1 History of the Refracting Telescope

The invention of the refracting telescope paved the way for modern lens design and optical engineering practices used today. The first refracting telescope, the Galilean or Dutch telescope, was comprised of a positive objective lens and negative eye lens. Credit is given to Hans Lipperhay for first constructing and demonstrating a working Galilean design in 1608. Evolving from the idea of spectacle lenses, the first refracting telescope created motivation which led to the development of other instruments such as: binoculars, microscopes, other variations of the refracting telescope, and ultimately the photographic lens. With Lipperhay demonstrating that, "All things at a very large distance can be seen as if they were nearby…" other scientists soon started proposing other solutions [2]. In 1611, Johannes Kepler proposed another common type of refracting telescope known as the Keplerian design, just three years after Lipperhay's demonstration [1]. His design utilizes both a positive objective and positive eye lens and was applied to astronomical viewing because the resulting image was inverted. These two variations of magnifying, afocal instruments led to a swift evolution of the original refracting telescopes to the modern designs known today.

However, there were still many issues that inhibited the performance and image quality produced by these telescopes. The most noticeable limitation in original telescopes was chromatic change of focus, which was the result of a single glass material focusing different wavelengths at different positions. Glass homogeneity, surface curvatures, and lens diameters were other factors responsible for degrading the image quality and resolution. In a letter that Galileo had written in 1616, he mentions that from a group of 300 lenses, only three were of high enough quality to be used in a terrestrial telescope and none could be used for astronomical telescopes [3]. As

materials became more consistent and techniques for grinding and polishing lenses improved, more defined aberrations became apparent and required correcting for.

1.2 Improvements to the Original Designs

From 1617-1662 much work was done on constructing and improving the performance of the Keplerian refracting telescope. This instrument initially produced an inverted image, making it unsuitable for terrestrial application. This time period was responsible for producing the erecting or relay lens, which produced an upright image and later, Huygens added the field lens to the eyepiece. These additional elements provided the Keplerian design with proper image orientation, sufficient magnification, and larger field of view [1].

The addition of these lenses were incorporated to improve the performance of refracting telescopes in terms of their field of view and magnifying power. However, more importantly, scientists started observing different phenomena relating to the image quality of these instruments. The observation and correction of optical aberrations started to become an important topic that was congruent with the development and optimization of the Keplerian telescope. Spherical aberration was one of the first of the optical aberrations described and observed in history and can date back to Roger Bacon in the 13th century [4]. Major contributions from medieval Islamic scientists such as Ibn Sahl and Ibn Al-Haythm led to Bacon first observing spherical aberration in spherical mirrors. Sahl and Al-Haythm's notions of how light refracts and the understanding of using spectacle lenses gave Bacon better insight to his observations [5]. Almost 400 years after Roger Bacon first elucidated his observations on

spherical aberrations, Johannes Kepler and Renee Descartes further describe spherical aberration in their *dioptriques* in 1611 and 1637, respectively. Descartes discusses in detail in Discourse 8 of his *dioptrique* that, "spherical lenses will not bring all divergent rays to a single focus." [6] He solves this problem stating that hyperbolic and elliptical curves can correct for this error, with a hyperbola being the preferred shape for precision optics.

The other aberration that mainly limited the quality and resolution of the image in the earlier development of refracting telescopes was longitudinal chromatic aberration. The dispersive properties of the glass used in the telescope objective lenses resulted in a chromatic change of focus, where different wavelengths had different focus positions along the optical axis. This effect results in having a color blur at the nominal focus of the objective lens, which can drastically reduce the image quality and angular resolution of the refracting telescope. The solution of achromatizing the objective lens with two different glass types was invented by both Chester Moor Hall and John Dollond in the mid-18th century and patented by Peter Dollond in 1758 [7].

Before the development of the achromatic objective, which utilizes the combination of a crown glass (low refractive index, low dispersion) and flint glass (high refractive index, high dispersion), the problems of chromatic aberrations were maintained by aperture size. With single glass objectives, aperture sizes were kept to around 13 millimeters in diameter to minimize the chromatic blur diameter. This is due to the prismatic effects upon a curved refracting surface. For a given surface radius, the larger the aperture becomes, the more influential the sag of that surface is. This directly relates to the amount of dispersion introduced, so by keeping the

objective diameter small, longitudinal chromatic aberration can be minimized.

The creation of the achromatic lens allowed for the diameters of these objective to be significantly increased to around 50 millimeters. A comparison between the diameters of earlier pre-achromat and post-achromat objective lenses is shown in Figure 1. In the pre-achromat telescope it can be seen that the objective lens is much smaller, especially when compared to the barrel diameter of the telescope. While the achromatic objective is significantly larger and has a comparable diameter to that of the telescope barrel.

Figure 1. Comparison of a pre-achromat refracting telescope objective (left) and an achromat telescope objective (right)

It is crucial to have a well-corrected objective lens in a telescope because this element is mainly responsible for the quality and resolution of the output image. The eye lens mostly serves the purpose of magnifying the intermediate image produced from the objective. So any aberrations created by the objective lens are directly magnified by the eye lens and degrade the final image. In regards to chromatic aberrations, the blur produced by chromatic change of focus is mapped to the final image and scaled by the system magnification.

Chapter 2

Dollond Telescopes

John Dollond (1706-1761), his eldest son Peter (1730-1820), and Peter's nephew George Dollond (1774-1852) became the most popular manufacturers of refracting telescopes in Great Britain dating from their exploitation of the achromat until the mid-1800's. Originally a silk weaver, John Dollond became well-versed in the theoretical aspects of astronomy and optics. His son Peter was not as experimental, but had great practical skill with making instruments that his father devised. After the passing of his father, Peter began working with his nephew George Huggins, who later changed his name to George Dollond. George had the skills of both John and Peter, having excellent mechanical skill and a strong theoretical background [8]. It is believed that the clocked telescope objectives that are the main focus of this report came from the George Dollond era.

The quality of Dollond telescopes became very well-known, which led to them becoming the royal opticians making telescopes for the British monarchs, which is often nicknamed the Dollond Century [8]. The Museum of Optics at the College of Optical Sciences at the University

of Arizona is home to many of these Dollond telescopes. Figure 2 shows a couple examples of Dollond Telescopes with achromatic objective lenses. The first is a four-draw telescope that dates back to around 1820, this was the most common style of telescope produced by Dollond. The second example is a single-draw achromatic night telescope, dating from around 1840. This unique telescope design features a large diameter draw that produces a large exit pupil that enhances its use for night viewing. However, it is considered a terrestrial telescope, for it contains an erecting lens assembly to correct the image orientation. This telescope is one of the telescopes found to have clocked elements in the objective.

a)

b)

c)

Figure 2. a) Four-draw Dollond telescope b)Single draw achromatic night Dollond telescope with a c) close-up of the detail of the inscription on the eye draw

Along with the optics behind these instruments being of high quality, the mechanical components are also very well designed and machined. The barrel and all of the lens cells were made from high quality brass and threaded very finely to smoothly connect all of the components together. Other artistic elements are also incorporated into their telescopes such as etchings of their name and where it was made, along with if it should be used for day and/or night objects. The night telescopes had larger eye draws, such that larger elements could be used in the eyepiece to allow for more light collection.

2.1 Clocked Telescope Objectives

Within the Dollond telescope century, some other very interesting features were applied to a few of their objectives. When trying to better understand the features and engineering behind all of the components within the telescopes, David Steed, working with the Museum of Optics collection as well as his own personal collection, noticed that some objective elements were "clocked" within their lens cells. This clocking involves having a groove placed inside of the objective's cell parallel to the optical axis and corresponding notches etched into the lenses. This

clocking allows the lens elements to be placed inside the objective cell in the proper orientation and restrict any rotational movement. Once the lenses were placed in the cell, a retaining ring would thread into the back side to keep them secure.

An example of the lens and cell components that make up these clocked objectives for an achromatic doublet are shown in Figure 3. Each lens has one main notch ground along the peripheral edge and smaller ticks towards one surface of the lens. The main notches line up with each other and fit into the groove of the cell. The smaller ticks serve the purpose of properly placing the lenses within the cell in the correct order. The number of ticks etched into the lens represents its order (i.e. the 1-tick is the front lens and the 2-tick is the rear lens, etc.) and the surface which the ticks are on represent the rear-facing surface.

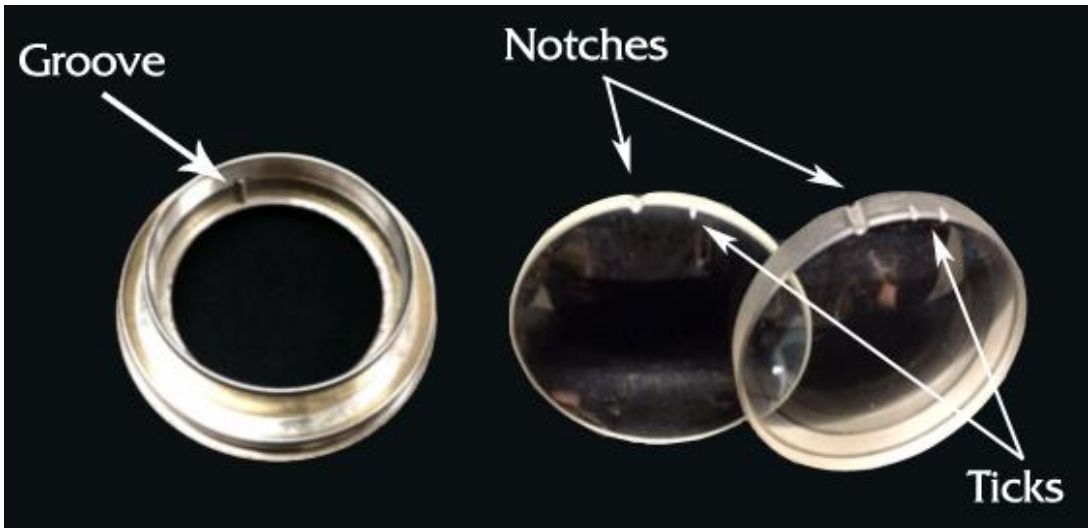

Figure 3. Clocked refracting telescope objective composed of a brass barrel with a groove and notched lenses

The purpose of the lens notches and cell groove is to properly align and restrict movement of the lenses once mounted. The presence of these features show that the designer purposefully wanted the lenses to be oriented in a particular direction with respect to each other. Making the groove

and notching the lenses was no easy task and required much time and effort, so it is presumed that there was some beneficial reason to doing this. The restricting of rotational movement between the two lenses led to the idea that it was to limit non-rotationally symmetric effects. Based on the natural astigmatic susceptibilities and difficulties associated with polishing the lenses, it was hypothesized by Grevienkamp and Steed that effects from surface astigmatism were trying to be minimized [1].

2.2 Controlling Astigmatism

Until the late 18th Century, the main effort in understanding optical aberrations was focused on correcting spherical and chromatic aberrations. Although chromatic effects were minimized with the development of the achromat, the effects of spherical and other aberrations were easily observed as mentioned by John Dollond in his 1758 paper to Rev. Dr. Birch. "However, the images formed at the foci of these object-glasses were still very far from being so distinct…in order to make the refractions in the required proportions, that they must produce aberrations, or errors, in the image, as great, or greater, than those from the different refrangability of light." [9].

Once the effects of chromatic and spherical aberrations were mitigated, other phenomena that had only briefly been observed became of great interest. Astigmatism had been noted decades prior to the development of the refracting telescope, but there was no solid understanding of this error. In the 17th Century, Isaac Barrow had initially determined the position of the tangential focus, with Isaac Newton later determining the sagittal focus [10]. The early 1800's resulted in a much deeper understanding and definition of the astigmatism aberration. Thomas Young first

made note and depicted tangential and sagittal imagery in 1801, observing that different sections of a beam come to a ‘nearer’ focus and ‘remoter’ focus [11]. The term astigmatism was later applied when G.B. Airy further observed, “…that the rays of light coming from a luminous point and falling upon the whole surface of the pupil do not converge to a point at any position within the eye but converge in such a manner as to pass through two lines at right angles to each other.”[12].

It is important to discuss the two common types of astigmatism: the Seidel aberration astigmatism (or third-order astigmatism) and axial astigmatism. Although the two arise from different conditions, the errors that are introduced to the wavefront are close to the same. Both result in different orthogonal meridional planes coming to focus at different positions along the optical axis. Seidel astigmatism occurs in off-axis ray bundles for rotationally symmetric systems. A pair of rays in the tangential plane strike the surface asymmetrically while a pair of rays in the sagittal plane strike the surface symmetrically. However, axial astigmatism is introduced by having different radii of curvature in orthogonal directions which results in the different focus positions. Axial astigmatism is the result of lens manufacturing and polishing errors and is inherent to the process due to the nature of shaping a surface. Toricity is introduced to the surface and is the reason why it is believed that the lens clocking was done to control this error. If the same optician polishing the lenses tended to introduce the same astigmatic shape to a surface during polishing, properly orienting the surfaces to each other could minimize if not eliminate the total effect.

Axial astigmatism can be thought of and represented similarly to Seidel astigmatism in terms of how it effects the wavefront. The amount of error introduced to the final image by third-order astigmatism (and defocus) can be represented in two ways: through its wavefront error coefficient or the ray error. The wavefront error W describes the exact shape of the wavefront deformation in comparison to a perfect reference wavefront and is shown through equation 1. Astigmatism has a quadratic dependence on field height H, normalized pupil coordinate ρ, and azimuth angle.

$$W = W_{222}H^2\rho^2 cos^2\theta + \Delta W_{20}\rho^2 \qquad \text{eq. (1)}$$

Similarly, the ray error describes how rays along the astigmatic wavefront deviate from the ideal image point produced by the reference wavefront. The ray error can be found by taking the derivative of the wavefront error with respect to both the y and x pupil dimensions: y_p or x_p. The ray errors associated with astigmatism are shown in equations 2 and 3 and express the interesting phenomena that occurs at different focus positions.

$$\varepsilon_y \propto -4(f/\#)y_p[W_{222} + \Delta W_{20}] \qquad \text{eq. (2)}$$

$$\varepsilon_x \propto -4(f/\#)x_p\Delta W_{20} \qquad \text{eq. (3)}$$

These expressions show how different object meridians of a lens have different amounts of ray deviation (aberration) from the ideal reference. Specifically, the sagittal and tangential planes from an object point will have different amounts of aberration introduced to the wavefront. Because the ray error introduced by astigmatism is dependent in only one linear dimension, it results in a line-shaped spot at each focus position. When the image plane is placed at the sagittal focus position (the defocus term ΔW_{20} equals zero), the ray error in the x-direction ε_x will be zero and the ray error in the y-direction $\varepsilon_y$can be found through equation 2. This results in a

linear spot at the sagittal focus in the vertical direction because the error is along the y-direction. Similarly, when the image plane is positioned at the tangential focus (the defocus term $\Delta W_{20} = -W_{222}$), the ray error will only occur in the x-direction resulting in a linear spot in the horizontal direction.

The same treatment can be applied to axial astigmatism, however there is no dependence on field height H. The wavefront error coefficient is expressed as W_{022} and has the exact same pupil position dependence, but the missing field height term results in axial astigmatism being present on-axis. In terms of wavefront degradation, axial astigmatism is comparable to spherical aberration in the sense that it will always be present in the optical system, but remain constant over the entire field of view. The different sources for third-order and axial astigmatism are shown in Figure 4 along with the resultant wavefront shape [13].

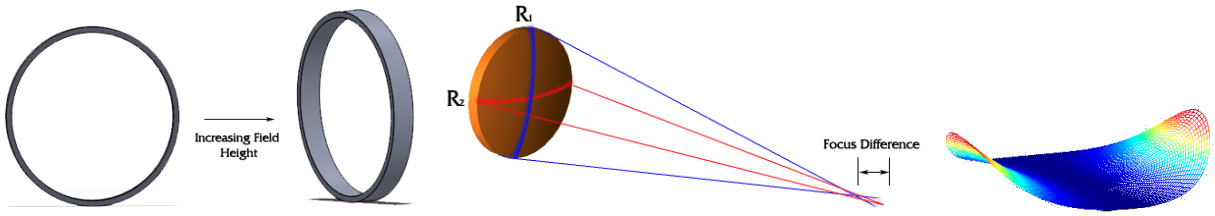

a) b) c)

Figure 4. Illustration of third-order astigmatism a) in comparison to axial astigmatism b) and the resulting wavefront from both c). As the field height increases and the object moves more off-axis, the shape of the aperture appears elliptical resulting in astigmatism.

2.3 Making the Objective Lenses

Although astigmatism can be derived from two different conditions, the resulting effects on the wavefront are the same. Based on the polishing techniques used in the 1800's, it is believed that

the astigmatism exists in the Dollond objective lenses from manufacturing slightly different optical powers or curvatures in orthogonal directions of the lens surfaces. The method of polishing lenses had been significantly improved from the 17^{th}-19^{th} Centuries but still resulted in some surface imperfections and non-symmetries. This reasoning, in addition to the naturally astigmatic tendencies that polishing a surface produces is what led to the belief that this is the reason that the lenses were clocked.

From the development of lens making for spectacles, polishing had always been an issue. Originally, lenses were polished by hand on a piece of rotating felt or deer leather. It was very difficult to polish the lens out to its entire diameter and the method of polishing introduced more and more asphericity and unevenness to the surface. Even obtaining the base spherical profile to a lens was no easy task until Sirtirus devised a method in the mid-1600's [14]. A grinding mold was first made by hammering metal to the roughly desired concave shape and then using a curved file to fine tune the profile of the sphere. Molten lead was then poured into the mold to produce a convex casted copy. The mold and cast were then ground together on a lathe to smooth out all irregularities between each surface, leaving a sphere with the desired radius which could be used to grind a convex or concave lens. Major breakthroughs in polishing did not appear until 1645 when Schyrl de Rheita and Johannes Weisel greatly improved the process [3]. Further perfections to the polishing process were made by the Italian, Giuseppe Campani and Englishman, Johannes Marshall, but were kept very secret and are still not fully known to this day. However, in Rheita's book he suggests using a special type of polishing paper glued to the spherical grinding surfaces for proper polishing [15].

The jump from making spectacle lenses to telescope objectives was also quite significant. When making lenses for use in spectacles, the active diameter used by the lens was much smaller because the aperture size defined by the eye was very small. In daylight, they eye has an aperture of roughly 2mm, so only a small portion of the lens needed to be of high quality. However, telescope objective lenses were much different. The entire diameter of the surface was needed and all irregularities present anywhere on the surface would degrade the image quality. Being able to properly polish larger sized lenses was not the only obstacle that needed to be overcome. The quality and homogeneity of the glass material used needed to be improved. When trying to optimize his telescope's performance, Peter Dollond had mentioned, "The difficulty of procuring good glass of so large a diameter, and the thickness required, in order to correct the aberration in such large apertures, has prevented me from attempting to extend them any farther." [16]. The improvements in both optical glass and polishing techniques resulted in some high quality instruments by the mid-1800's.

Chapter 3

Interferometric Testing

To test the hypothesis that minimizing astigmatism was the main reason behind the clocking efforts, a variety of tests were performed on the objective lenses. Surface and transmision tests were performed to obtain the interferograms and wavefront maps. With this information, the individual aberrations contributing to the total optical path difference were obtained to determine the largest contributors. A WYKO 6000 fizeau interferometer manufactured by WYKO in Tucson, AZ was used to record data in conjunction with 4Sight software, provided by 4D Technology in Tucson, AZ to analyze the wavefronts.

The three different notched objectives made by Dollond were tested to confirm that the results were consistent. Each telescope objective was catalogued by the Museum of Optics at the College of Optical Sciences at The University of Arizona. The three objectives are compromised of two achromatic doublets and one apochromatic triplet. The two doublets are labeled T21 and T59, and the triplet is labeled T70. An image of the T59 objective can be seen in Figure 5 below. All of the objectives are similar in size and design; the cell has a T-shaped cross section with the threads for attaching to the barrel being on the outermoust edge.

Figure 5. T59 objective mounted in the telescope barrel and alone in its cell

3.1 Transmission Testing

The most applicable analysis performed on the objective lenses was a transmission test to observe the output wavefronts. Transmitted wavefronts were analyzed with the lens notches at different orientations with respect to each other. If the lens clocking was intended compensation for astigmatism, then in the 0° orientations, the astigmatic errors of the two elements would at least be partially cancelled. At the 90° orientation, the astigmatism on the surfaces would then add and a greater amount of transmitted astigmatism would result in the wavefront. The test required removing the lenses from their brass cells and securing them in a different mounting apparatus. This mount was composed of a self-centering lens mount attacthed to a goniometer rotation stage to control lens orientation. Thin foam was wrapped around each contact point on the self-centering mount to account for any slight deviations in lens diameters. The foam material was able to deform and keep both elements secure and centered in the mount.

Once mounted, the rear element was kept fixed with the notch oriented vertically and the front element was rotated. For the T70 triplet objective, an additional orientation was tested and will be discussed in more detail later. The orientation of the front lens' notch was then used as

notation and reference for the experiments. When both notches were aligned vertically, this was referred to as 0° (offset between notches) and having the front lens' notch oriented orthogonal to the rear lens was referred to as 90°. Figure 6 shows the testing setup for the testing configurations.

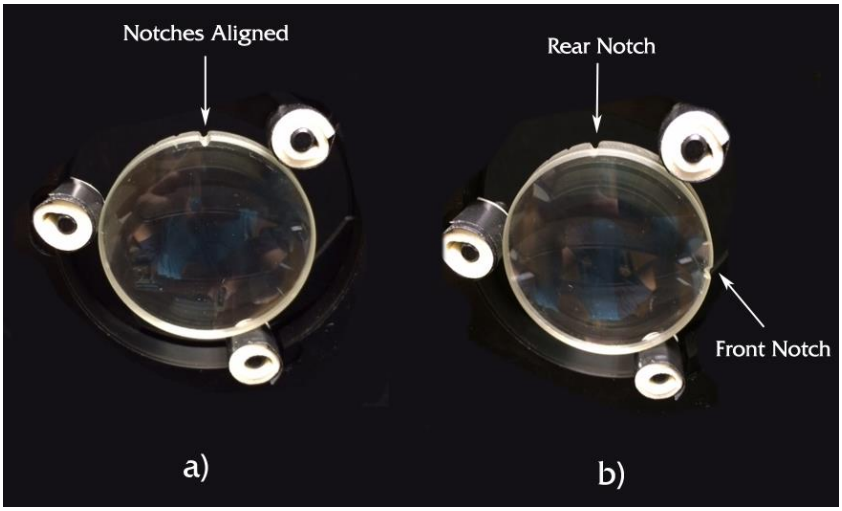

Figure 6. Lens orientations for 0° offset (a) and 90° offset (b)

The objective lenses were tested in double pass for the transmission measurements. A depiction of the setup for testing the lens in transmission is shown in Figure 7. Collimated light produced by the fizeau interferometer passed through a transmission flat to create a reference beam. After exiting the interferometer, the light passed through the objective under test and was focused down to a point. A very precise steel ball bearing was then placed concentric with the focal point of the objective to retroreflect the beam back through the lens and into the interferometer. Being a sphere made with high precision and tight tolerances, the steel ball bearing served as good retroreflector for the transmission testing. This was the optimal test setup because it replicates how the telescope obective was designed and meant to be used: with collimated light incident on the front surface.

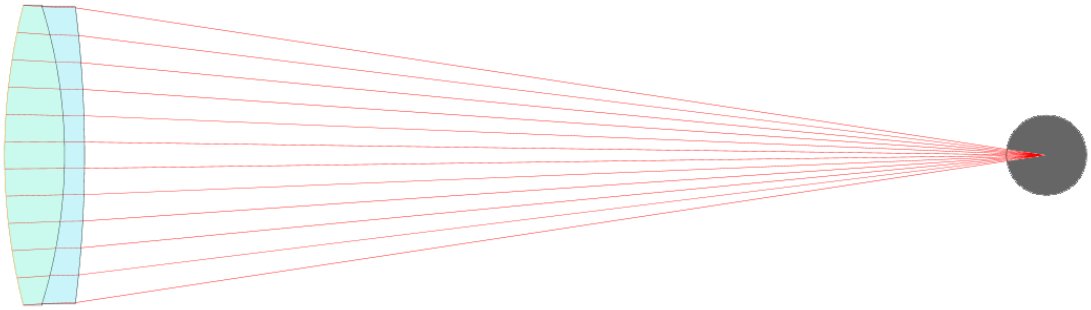

Figure 7. Schematic for the transmission test performed on the telescope objectives

A variety of different data values were looked at to observe the effects of rotating the lenses away from the nominal clocked position.The wavefront error maps were looked at to visually inspect any differences in the optical path between the orthogonal orientations. These interferograms served as an aid to notice if there were any double-plane symmetries present, which are congruent with astigmatism. Both the peak-to-valley and RMS wavefront error values were taken to quantitatively diagnose the wavefronts. Lastly, the values for the astigmatism coefficients were taken and plotted to observe the differences in the magnitude of astigmatism between different orientations.

3.1.1 Interferograms

The OPD maps serve a useful purpose of providing a visual of the wavefront after transmission through the objective similar to a contour map. With the interferograms obtained, it is typically easy to quickly diagnose the main aberrations present in a system. If astigmatism is the only aberration present or it greatly dominates the system, the resulting wavefront map will have a double plane symmetry or saddle appearance. This shows up as high spots in one linear direction and low spots in the orthogonal linear direction. When other aberrations are present but their magnitude does not compare to that of astigmatism, an elliptical shape will be present. However, the wavefront maps can become very complex when the magnitude of other aberrations are

comparable to that of astigmatism. If this occurs, the individual aberration terms must be identified to properly determine what is occuring.

Figure 8 shows the resulting interferograms for the three refracting telescope objective T21, T59, and T70. When post-processing the data some aberration terms were subtracted from the measured wavefront. Piston, tilt in both x and y-dimensions, and power were removed from the captured data. These terms were able to be removed because they are a result of the alignment of the objective lens with respect to the interferometer. It is important to note that while aligning the objectives, adjustments were made to null the interference pattern. However, there was still the possibility of positioning the reference sphere slightly out of focus or having some residual tilt leftover which are contributions from the testor and not the objective lenses. The following wavefront maps plot the data that was obtained to a 24-term Zernike fit. Using this fit to the data helped remove etalon effects that were observed in some of the interferograms. The closely matched curvatures between surfaces in contact produces a Newton's ring effect that could be seen in the interferograms but did not effect the aberrations in the transmitted wavefront.

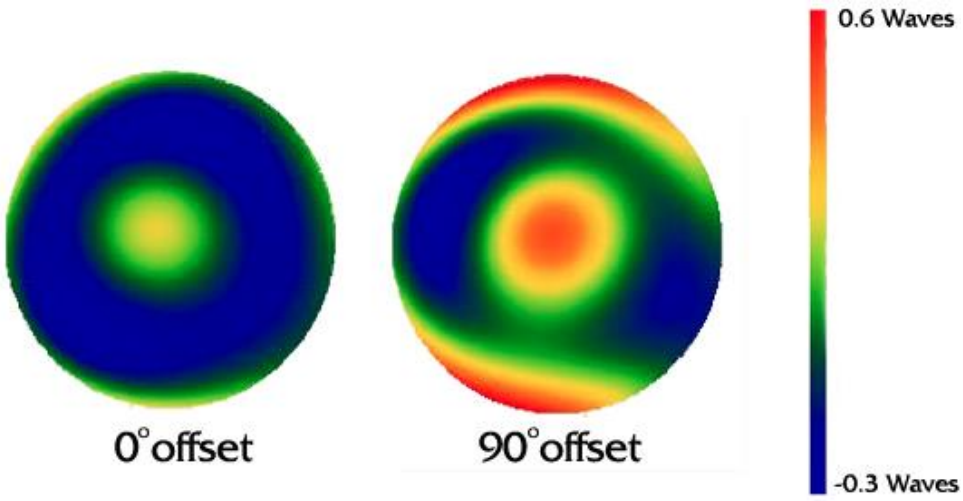

a)

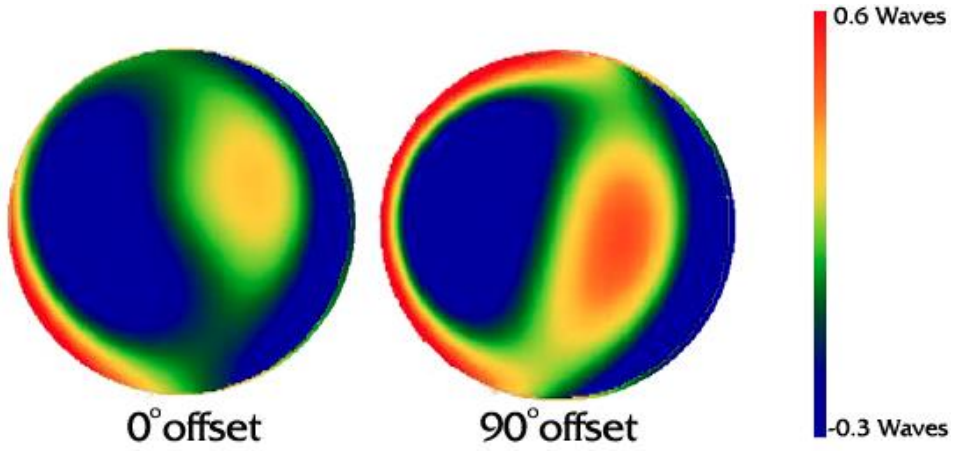

b)

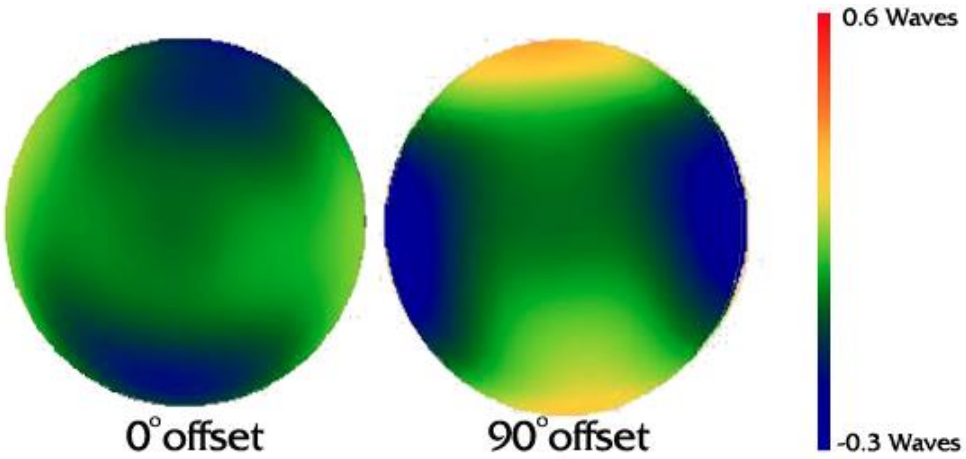

c)

Figure 8. Transmitted wavefronts from the T21 doublet (a), T59 doublet (b), and T70 triplet (c)

Review of the wavefronts produced by each objective show some interesting phenomena. The interferograms from the T70 objective in Figure 8(c) express that this lens is mostly dominated by astigmatism. With the notches lined up and no rotational offset between the two lenses, the saddle shape in orthogonal directions is minimal, but visible. When rotating the front element by 90° and crossing the lenses, the amount of astigmatism is noticeably increased and the double-plane symmetry is very noticeable. The interferograms for the T21 objective in Figure 8(a) also show an astigmatic shape when crossing the lenses. With the notches aligned there appears to be a minimal amount of spherical aberration, but when in the 90° orientation, the elliptical shape is

clearly visible. This is additional evidence that rotating the notches relative to eachother plays an important role in controlling and minimizing astigmatism. However, the transmitted wavefronts produced by the T59 objective are not so easily distinguishable. This doublet had larger amounts of coma present with magnitudes comparable to that of astigmatism. This resulted in a more complex interferogram that required looking at the individual aberration coefficients to better understand what was occuring.

To look at mostly the astigmatism present in the T59 objective, coma was further subtracted from the data and the differences from Figure 8(b) were observed. This is shown in Figure 9 and matches the expected trends. Although these interferograms show the desired results, it is not a truly accurate representation of the transmitted wavefront because the coma was removed. The 90° offset interferogram in Figure 8(b) does show an increase in the amount of wavefront error, which can be attributed to the change in astigmatism, but this is only clear when looking in Figure 9. The amount of astigmatism is significantly greater in the 90° offset position, but the comparable amounts of coma mask the distinctiveness in the transmitted wavefront.

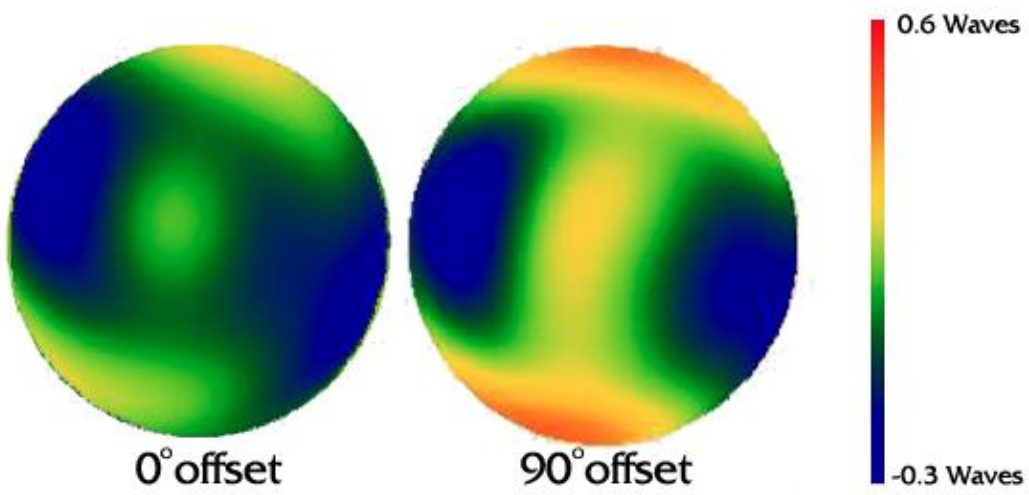

Figure 9. Transmitted wavefront from the T59 objective with coma subtracted

3.1.2 Wavefront Errors

The interferograms provide a nice visual diagnosis of what is occuring with the clocked lenses, but to quantify the exact effects on the wavefront, further numerical analysis was required. Both the RMS and peak-to-valley wavefront errors were measured to compare the deviation from a perfect reference sphere. For this experiment, the RMS wavefront error is more applicable since it provides an average of the oscillations and errors inherent to the real wavefront. Figure 10 plots the RMS wavefront errors for the three telescope objectives for both notch orientations. These results show significant improvements to the overall transmitted wavefronts of the objectives when the notches are lined up with no rotational offset. The T70 objective shows the greatest improvement, with the RMS error being doubled when the lenses are crossed. The interferogram in figure 8(c) showed that this particular objective is dominated by astigmatism, so by aligning the notches correctly, the astigmatism is reduced and the total wavefront error is also greatly reduced.

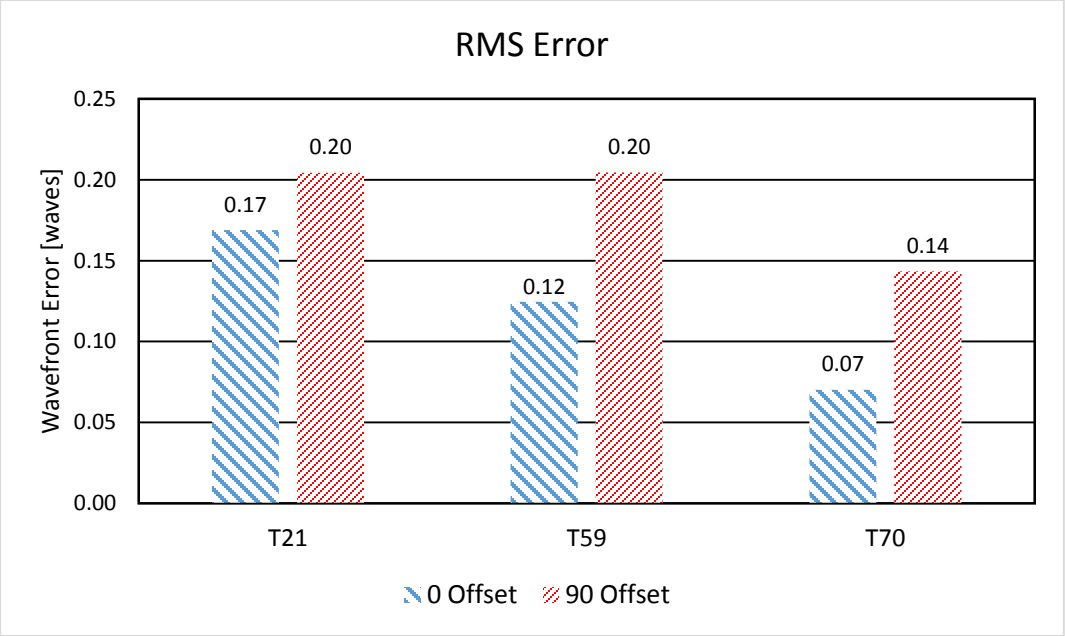

Figure 10. RMS wavefront errors for the three objectives

The peak-to-valley wavefront error for each of the objectives plotted in Figure 11 shows comparable results. The values are now increased becase one high data point and one low data point can drastically influence these results. However, the ratios between the aligned and crossed orientation for each objectives are similar to the RMS wavefront error results.

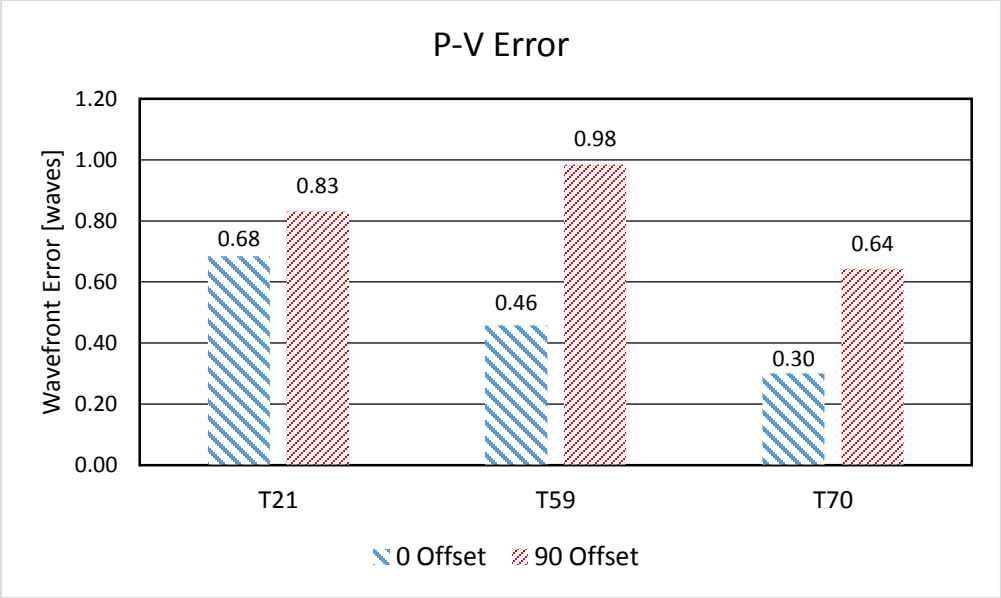

Figure 11. Peak-to-Valley wavefront errors for the three objectives

3.1.3 Astigmatism Values

The last set of data that was focused on were the individual astigmatism values from each measurement. The previosuly mentioned interferograms and wavefront errors take all of the aberrations intrinsic to the telescope objectives into account. With the propsed reasoning behind clocking the lenses being to control astigmatism, these values were of the most interest. Figue 12 shows the third-order astigmatism coefficient values for the three objectives in each orientation. With the notches lined up, it was expected that astigmatism would be minimized. Thus by rotating one element by 90° and crossing the lenses, the amount of astigmatism that was being subtracted would now add to the total wavefront, doubling in magnitude. An example to further clarify the additive/subtractive property can be shown through some arbitrary axial astigmatism values. If the axial astigmatism introduced by the one element is represented by A_1 and the astigmatsim from the second element is represented by A_2, two equations expressing the 0° and 90° orientations can be used to solve for each. The value for minimal astigmatism obtained in the 0° orientation can be represented as $A_1 - A_2$, with the maximum value in the 90° orientation being $A_1 + A_2$. Some simple algebraic maipulation results in the 90° orientation astigmatism value being a function of $2A_2$, which is the source of this doubling in magnitude. The results obtained in Figure 12 closely match this trend, where having the lenses in the crossed orientation results in double the amount of astigmatism.

It was not expected that the amount of astigmatism would go completely to zero with the notches aligned in the nominal orientation. This can be a result of many factors with human error being the most likely. Since axial astigmatism is a result of manufacturing errors from the hand polishing process, the amount introduced is often not repeatable. The exact amount of astigmatic

error polished into one surface can not easily be replicated into another surface. The curvature of a surface can also influence how much astigmatism is introduced. Polishing a surface with a small radius of curvature in comparison to a large radius of curvature can result in a nonuniformity of axial astigmatism between the two. The shape of a surface can also further play a role in added diffulties to the manufacturing. Polishing a convex or concave surface can introduce other inconsistincies that add to the randomness of induced astigmatism.

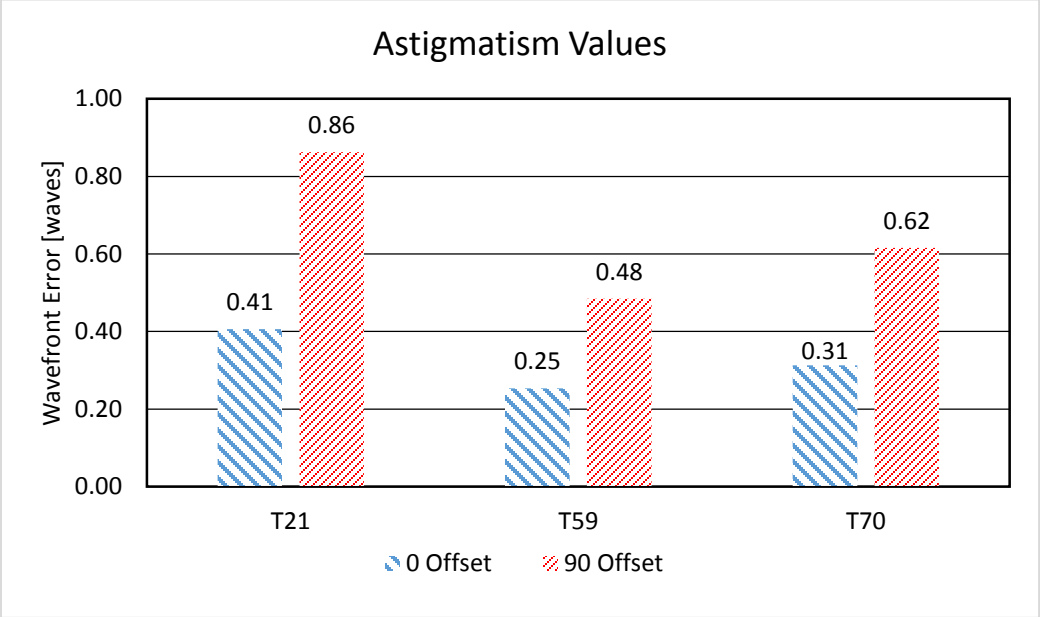

Figure 12. Values for the Seidel astigmatism coefficients

The net angle of astigmatism for each case was also found to see how the direction changed in addition to the magnitude. Table 1 shows the resulting angles of astigmatism for the different orientations. Interestingly enough, no trend between the angle of astigmatism was noticed between orientations. The T21 and T71 objectives show that the astigmatism orientation rotates by roughly 90°, but the T59 objective shows almost a 180° rotation between the two lens orientations.

	T21	T59	T70
0° Offset	-130°	40°	-70°
90° Offset	-230°	-120°	280°

Table 1. Net orientations for astigmatism in the telescope objectives

3.1.4 T70 Achromatic Triplet

The T70 telescope objective was an apochromatic triplet lens and therefore had an additional lens orientation tested to observe the effects. Initially only the front element of the triplet was rotated to observe the resulting effects and is described in the previous sections. Tests were also performed with rotating the front two elements, or equivalently rotating the rear element observe how the astigmatism changed. The results that were obtained were surprising because it showed that misaligning the rear lens did not have much of an impact on the total amount of astigmatism or wavefront error.

Figure 13 shows the interferogram for the wavefront when the rear element was rotationally offset by 90°. When comparing this to the wavefront OPD map in Figure 8(c) with all of the notches lined up in the nominal position, the two are very similar. The magnitude of astigmatism does not appear to change much, only the orientation changes by 90°. These results show evidence that the third element in the triplet is not astigmatic and that the balancing of astigmatism is mostly accomplished by the front two elements. Further evaluation of the surface data provides support to this theory.

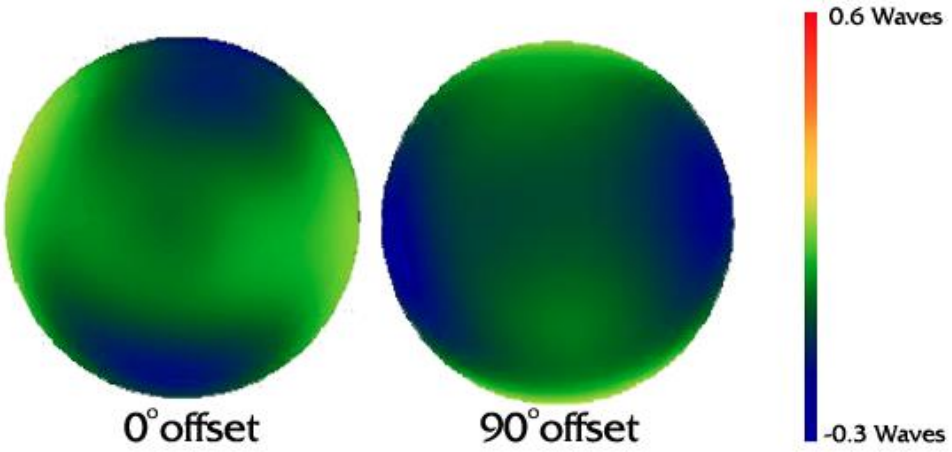

Figure 13. Transmitted wavefront for rear element of the triplet rotated with a 90° offset

A comparison of the wavefront errors and astigmatism coefficients further prove that rotation of the rear element is not as sensitive as the front. Figure 14 plots the wavefront errors for the three different orientations tested with the T70 objective. The RMS wavefront error remains unchanged with the rear element rotated with the peak to valley showing a slight increase. Because the peak to valley is an absolute measurment of the maximum and minimum wavefront, the small change is insignificant.

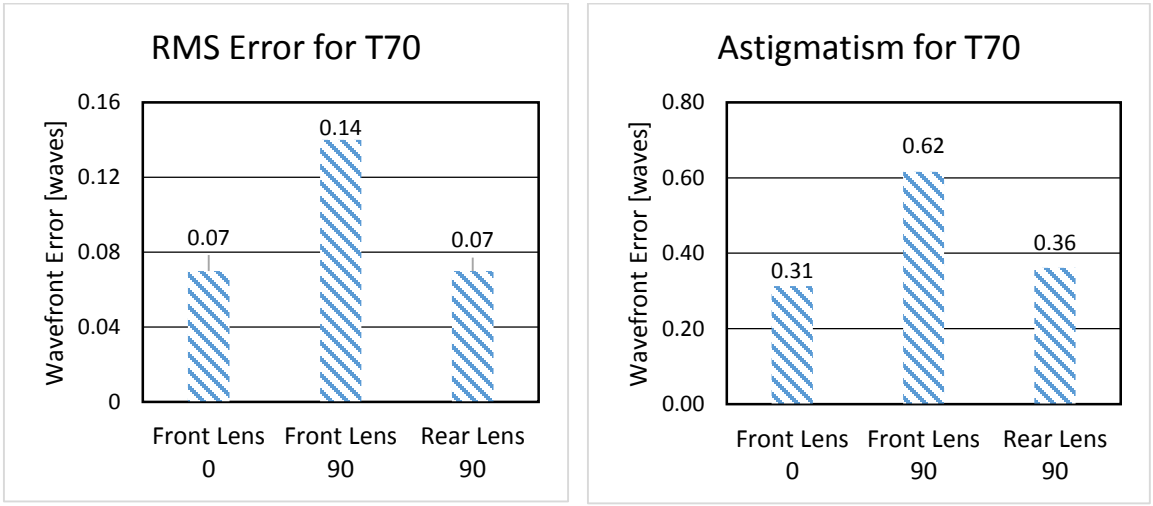

Figure 14. Wavefront errors for rear element of the triplet rotated with a 90° offset

3.1.5 T21 Objective Mounted in its Cell

To ensure that the cell itself and mounting configuration used for the interferometric tests did not introduce any astigmatism or additional aberrations, a few other measurements were made. The transmission test was performed with the T21 objective mounted in its cell with the retaining ring tightened as much as possible. It was considered that the force applied on the objective from the retaining ring may introduce more astigmatism than what was measured, thus making the clocking meaningless. Additionally, it is import to ensure that the measured amount of astigmatism was not introduced from the self-centering mount used for the interferometric tests.

Figure 15 shows the measured interferogram with the T21 objective mounted in its cell compared to the results obtained with the elements mounted in the self-centering mount. It can be seen that there is a slightly larger amount of spherical aberration present with the lens mounted in its cell, but that the amount of wavefront error does not appear to increase, and no additional astigmatism is introduced.

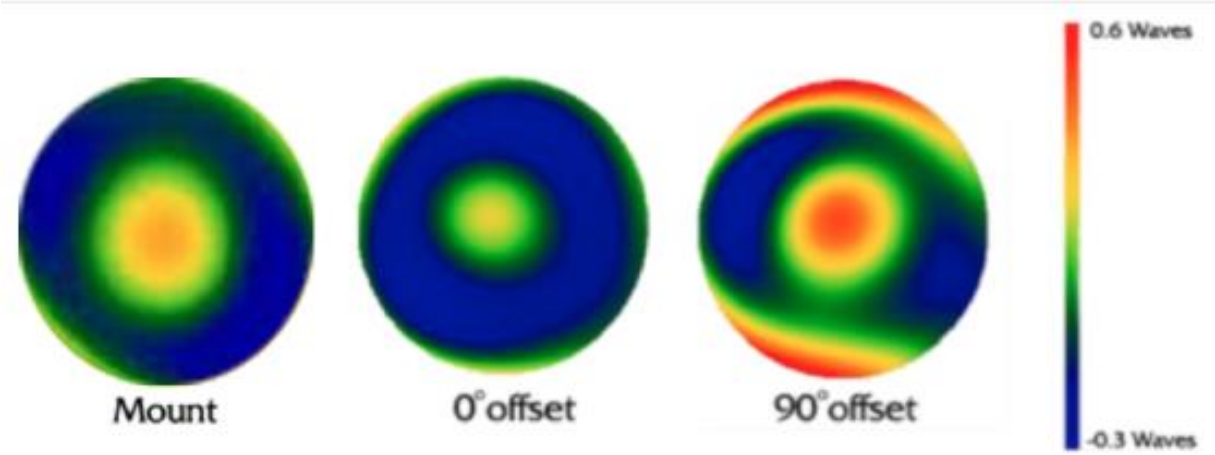

Figure 15. Comparison of the interferograms for the T21 objective with it mounted in its cell and in the self-centering mount for both notch orientations

Further inspection of the wavefront error values and astigmatism coefficients shows that neither the force from the retaining ring or self-centering mount introduce additional aberrations. Figure

16 plots the wavefront error and astigmatism coefficients for the T21 objective with the elements mounted in the cell. Again, when compared to the other measurements it is observed that neither mounting method introduces a significant amount of additional aberrations to the objective.

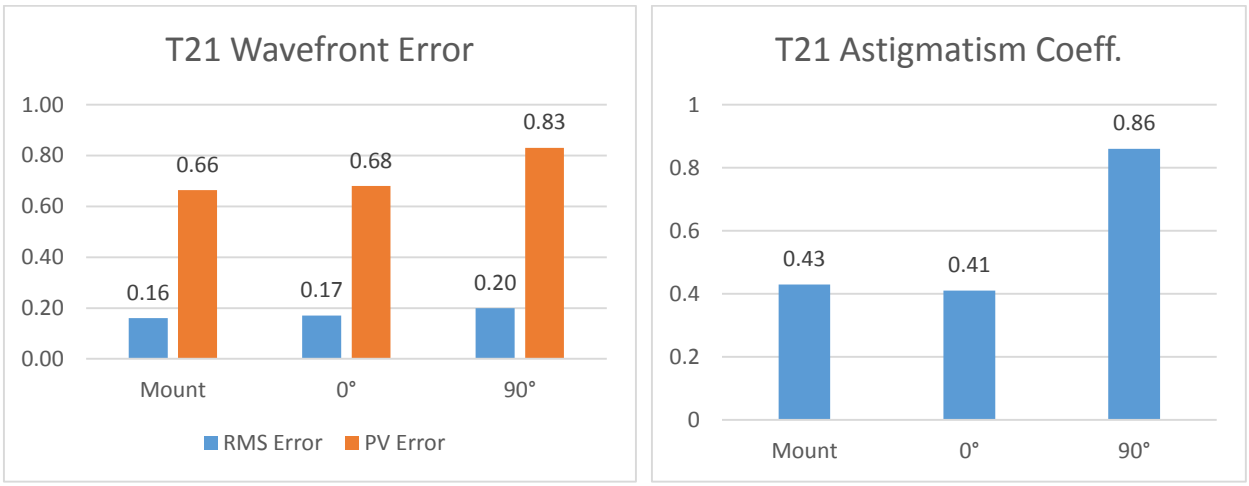

Figure 16. Comparison of wavefront errors and astigmatism coefficients for the T21 objective with it mounted in its cell and in the self-centering mount for both notch orientations

As another merit of visual inspection, crossed polarizers were used to observe any stress introduced to the elements from both mounting methods. To perform this test, one state of linear polarization was transmitted through the front of the objective and another linear polarizer oriented orthogonal to the front polarizer was used to analyze the transmitted light. These results are shown in Figure 17. It is easily observed that there is no stress at the contact points from the self-centering mount or retaining ring. If any mechanical contact point was applying a significant amount of force to the lens, the polarization state of the incident light would change and be noticeable when looking through the secondary analyzing polarizer.

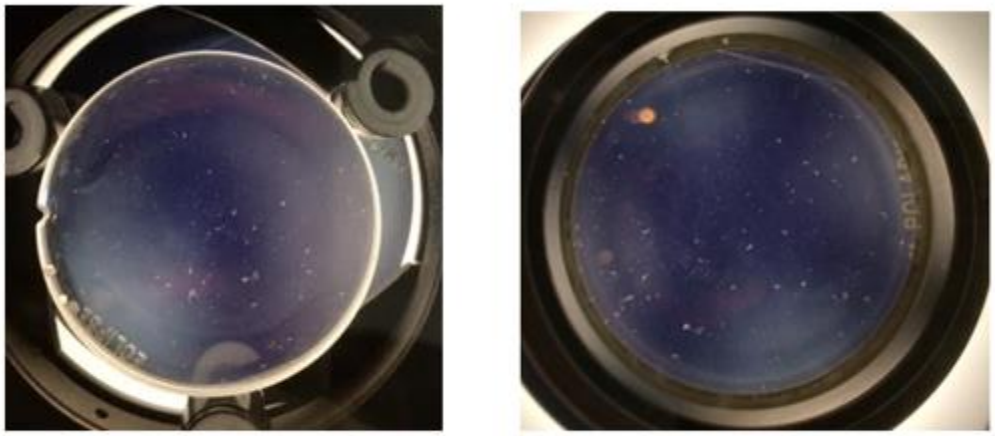

Figure 17. Crossed polarizer test for the T21 objective in the self-centering mount and its machined brass cell.

3.1.6 Coma Values

To confirm that astigmatism was the main aberration being controlled by the clocking efforts, the coma coefficients were also plotted. These are shown in Figure 18 and appear to display no common trends among the three objectives. In the T21 objective, the amount of coma reduces when the notches are rotated while it increases in the other two objectives. The percent change between each orientation also do not show any trends. This is hypothesized to derive from the anti-symmetric properties of coma. Half of the wavefront error is positive while the other half is negative, making the resultant combinations non-trivial, especially if the magnitude of coma in each element is not comparable. It is also quite possible that the inconsistencies in coma values are due to alignment errors.

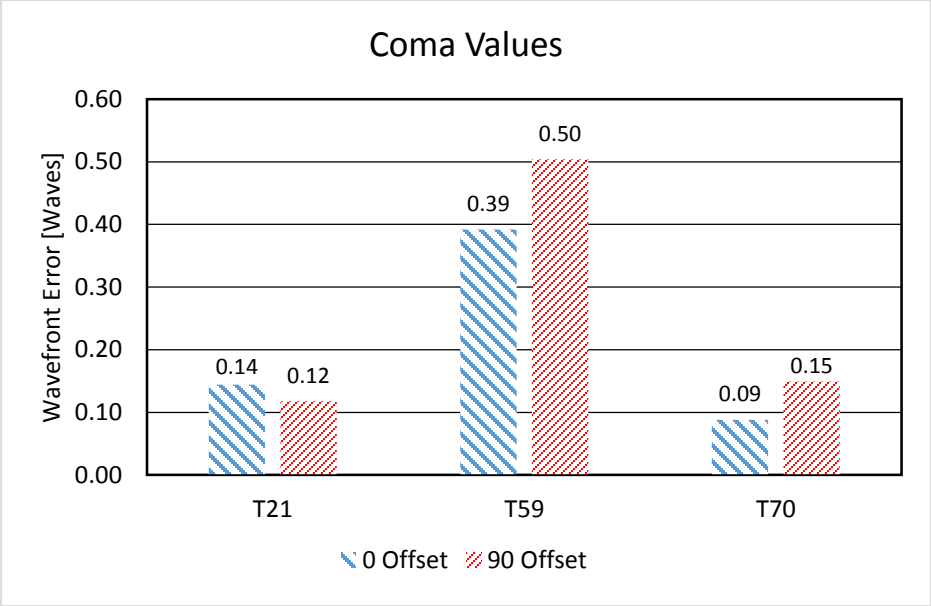

Figure 18. Values for the Seidel coma coefficients

3.2 Surface Testing

The individual surfaces of each lens were also measured to observe any trends between the different objectives. Using the interferometer in a reflection-test configuration, every surface of the of the objectives were characterized. A depiciton of the surface test setup is shown in Figure 19. It involved using a transmission sphere to focus the light exiting from the interferometer down to a point along the optical axis. The surface under test was then positioned inside of the focusing beam at the location where its radius of curvature was concentric with the transmission sphere's focal point. Fresnel reflection from the lens surface retroreflect the beam back into the interferometer and the resulting interferograms are obtained. In the case of a concave surface, the surface must be placed past the focal point of the reference sphere so that its radius can match the wavefront based on sign convention.

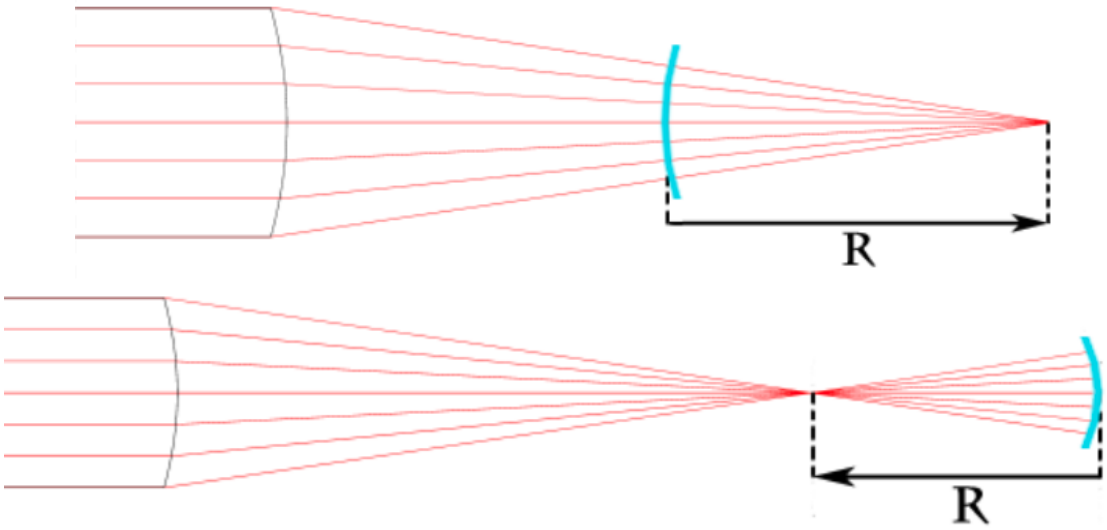

Figure 19. Schematic for the surface test performed for both a convex and cooncave surface

While performing the surface tests, the radius of each surface was measured. This was accomplished by first placing the surface at the cat's eye postion and then moving it along the optical axis until its radius was concentric with the interferometer's beam (at the measurement acquisiton location). The difference in the two positions was equivalent to the radius of curvature for the surface. This value was then used to calculate the 'f-number' for the surface to try and match it to the closest transmission sphere f-number. An arbitrary transmission sphere of F/7 was first used to measure the radii for each surface and calculate their f-numbers, the calculated f-number was then best-matched by the available supplies. The importance of matching the f-numbers is so that the lens aperture is properly filled. When measuring the surfaces of each element, it is better to overfill the aperture rather than underfill. That is so the entire diameter of the element can be measured. With the max amount of aberrations occuring at the edge of a surface, overfilling the pupil provides a full characterization of the surface. Table 2 shows that measured radii for each surface and the corresponding f-numbers. The available transmission spheres had f-numbers of F/1.4, F/3.2, and F/7 which were used for surface testing.

	Surface	Radius [mm]	f/#		Surface	Radius [mm]	f/#		Surface	Radius [mm]	f/#
T21	1	79.5	2.0	**T59**	1	78.7	2.0	**T70**	1	208.6	5.2
	2	-91.6	2.3		2	-91.9	2.3		2	-129.3	3.2
	3	-91.6	2.3		3	-91.9	2.3		3	-129.3	3.2
	4	-206.9	5.2		4	208.0	5.2		4	175.5	4.4
									5	175.5	4.4
									6	-415.8	10.4

Table 2. Measured radii of curvature and calculated f-number for each surface

The values presented in Table 2 show strong consistencies between the T21 and T59 objectives in terms of their manufacturing. Both objectives come from the same telescope design, being single draw achromatic night telescopes with near identical dimensions. The two objectives have similar radii of curvature for each surface, with slight variations most likely arising from manufacturing tolerances and/or meaurement tolerances. However, the interferograms produced by each objective for each show signifigantly different aberrations present. This further shows how much of an art form polishing the surfaces was. The base profiles for each surface can repeatedly be ground using the aforementioned techniques in Section 2.3, but polishing required much greater skill.

Figure 20 shows the surface profiles for all of the lens elements in the T21 and T59 objectives. The views for each surface interferogram are presented in corresponding aperture locations. This refers mostly to the rear surface for both elements; the left side of the images directly correspond to the left side of the lens. The surface data is presented in such a way as to simulate all of the surfaces being lined up – a ray passing through the assembly will go through approximately the same x-y coordinate on the surface maps. When measuring the rear surfaces, the lens was flipped from left to right by 180°. This required reflecting the measured interferograms about the vertical axis to properly obtain the correct lens orientations. The negative surfaces also required

additional reflecting about the horizontal axis to properly orient the top and bottom of the surface. Since these measurements were made past the focus from the interferometer's reference sphere, the location on the surface aperture being measured was inverted.

The results from the surface profiles can be interpreted in two different ways. The images display the reflected wavefront created by each surface, so any variation can be atttributed to the deviation from a perfect reference wavefront. However it is also possible to relate the reflected surface wavefronts to different thicknesses across the surface. The high zones on the surface maps are produced from an increased thickness in that particular region of the surface, which results in that region being slightly closer to the interferometer aperture. Likewise, the low zones can be thought of a decrease in thickness in that particular surface region.

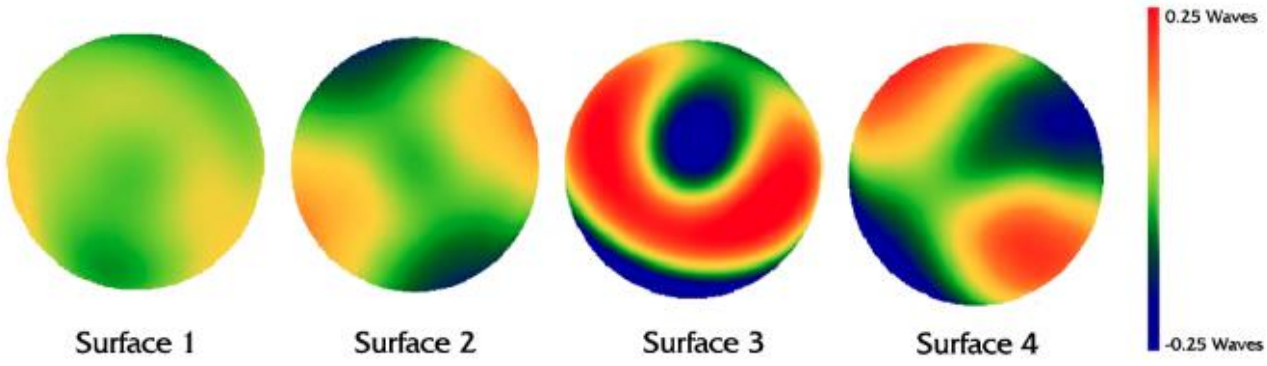

a) T21 Objective

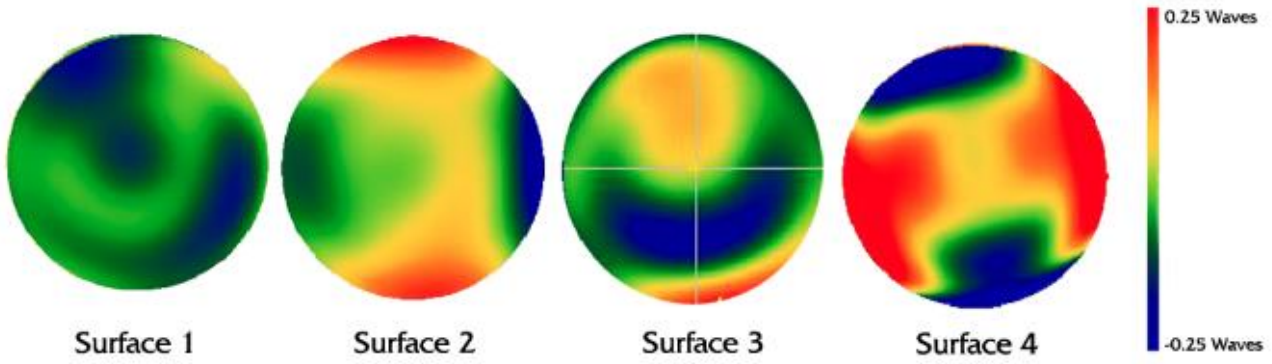

b) T59 Objective

Figure 20. Surface maps for the T21 a) and T59 b) objective lens elements

These images show that the rear surfaces of both elements are astigmatic, with surface 4 contributing the most astigmatism. The double plane symmetry can be observed in both surface 2 and surface 4, with the magnitude appearing the largest in the rear-most surface. From these results, it inferred that polishing the rear surface of the lens elements, especially of the negative elements, was more difficult. The grinding and polishing techniques described in Section 2.3 worked well for lenses with one planar side to secure. But when trying to polish an additional curved profile to a lens, the precision could not be obtained.

The surface profiles for the T70 triplet lens show similar trends to the doublet but also some other interesting results. Figure 21 plots the measured surface height errors for the three elements in this telescope objective. The transmission test results previously showed that rotating the rear element of the triplet did not have much of an influence on the astigmatism control. Looking at both surfaces of the rear element clearly show why this was the case, there was no apparent astigmatism in this lens. The front two elements are comparable to those in the T21 and T59 objective, with the rear surfaces being astigmatic. The front surfaces have mostly spherical aberration intrinsic to them with the negative surface (surface 3) having a higher amount of wavefront error. However, the rear element of the triplet is dominated by spherical aberration in both surfaces. The profiles for surfaces 5 and 6 show close to equal and opposite amounts of spherical aberration present, which helps keep the total transmitted wavefront error low because the sum of aberrations in both of the surfaces is close to zero. This is interesting because it shows evidence that it was possible to polish the rear surfaces of the lens in a rotationally symmetric manner.

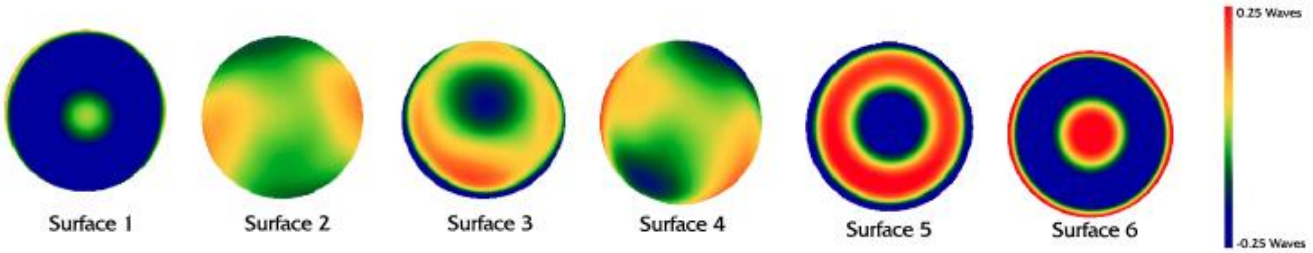

Figure 21. Surface maps for the T70 triplet objective

3.2.1 Computer Model

A computer model of the T21 objective also was designed to observe if the simulated wavefront data compared to the actual measured data. The radius for each surface and element thickness were measured and imported into Zemax to model the doublet. Nominal refractive index values for crown and flint glass of 1.5 and 1.58 were assumed for each element and used in the Zemax model. The transmission test performed in Section 3.1 was then simulated in the software and the wavefront at the image plane was plotted. For the model, each surface was modeled as an irregular surface so that individual aberrations can be applied. The Seidel coefficients obtained from the surface measurements above were applied to each surface to replicate the T21 objective. It is important to note that when Zemax requires the aberration values to be defined in waves. The 0° and 90° orientations were achieved by definining the *angle* cell for the respective orientation, this rotates the surface with respect to the y-axis. The simulated transmitted wavefront produced by Zemax and the actual measured wavefront for both lens orientations are shown in Figure 22.

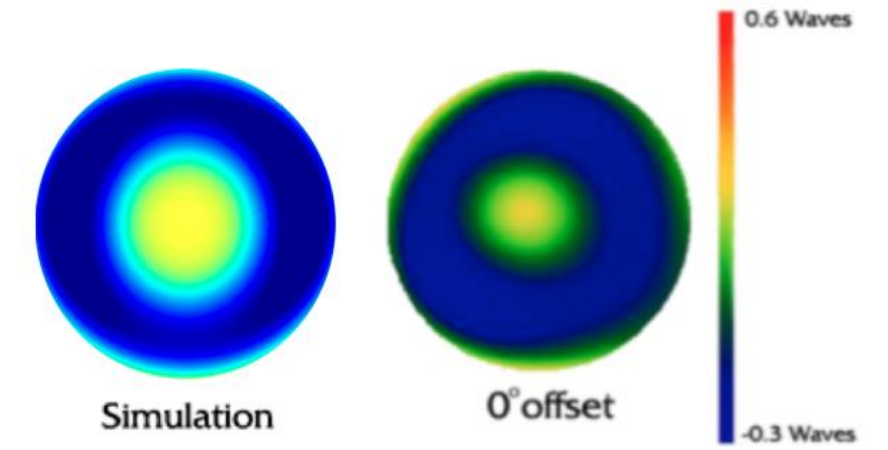

a)

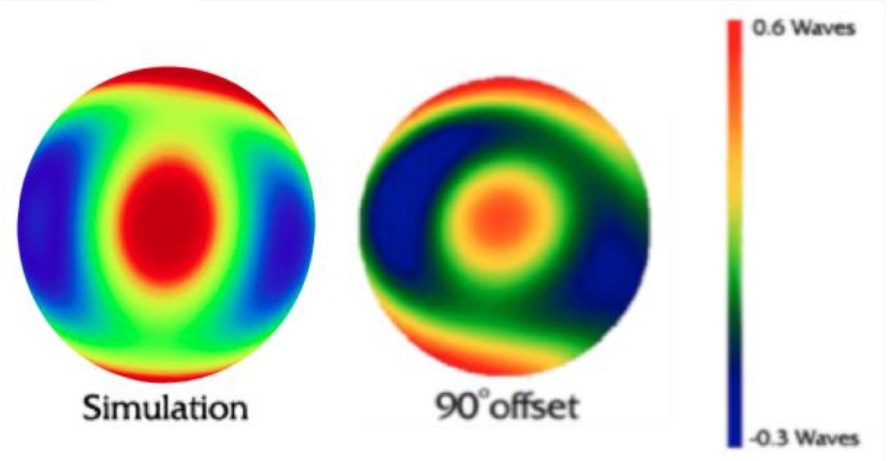

b)

Figure 22. Simulated wavefront compared to the measured wavefront for the T21 Objective in the a) 0° orientation and b) 90° orientation

Both the shape and magnitude of the simulated interferogram closely resembles the results obtained from the transmission test. The simulated wavefronts in both orientations are consistent with the measured wavefronts. The simulation for the 0° orientation shows slightly more spherical aberration, having a larger core in the center. But the magnitude of both the simulated and measured are consitent with each other, having a peak-to-valley error of around 0.7 waves. The simulated results for this orientation required some post-processing to take care of a piston effect, which was performed in Matlab. The colormap of the Matlab plot was shifted to adjust for the constant piston offset and properly center the simulated data. The simulation for the 90° much more closely relates the measured wavefront, having a central, circular high spot

associated with spherical aberration with a surrounding elliptical low zone intrinsic to astigmatism. The upper and lower edges also reflect a peak in the transmitted wavefront, which is apparent in the mesured data. The wavefront error values are also fairly consistent with each other. The simulated wavefront has a peak-to-valley wavefront error of 0.86 waves, which closely matches the measured peak-to-valley wavefront havng an error of 0.83 waves.

3.3 Star Testing the Objectives

The last test performed on the objectives was a star test to qualitatively diagnose any astigmatism present. Not having any metrology instruments to test these lenses in the 19th century, it is speculated that a star test was performed on the objectives to test the image quality and to orient the lenses and provide the correct clocking. The Foucault and Ronchi tests which are commonly performed on teles cope optics were not developed until 1858 and 1923, after Dollond manufactured these objectives. To get the proper orientation of each element, it is believed that the optician making these particular telescope objectives would rotate one of the elements until the resultant image was of the highest quality, thus minimizing astigmatism. This is only speculation, we are unaware of any descriptions in the literature describing the process that was used to determine the desired clocking.

To replicate this, an experimental star test was performed inside of a laboratory. The setup is shown in Figure 23 and involved building a beam expander using a spatially filtered He-Ne laser with a 5 micron pinhole to act as the point source/star. The collimated light was then focused down by the telescope objective to an intermediate image, which was then magnified by a 40X microscope objective and projected onto a viewing screen [17]. The microscope objective was

moved slightly in and out of focus and the resulting spot patterns were observed. Photographs were then taken of the resulting images on a viewing screen.

Figure 23. Lab bench setup for the simulated star test

With the notches aligned in the 0° orientation, no significant asymmetric observations were made while moving the microscope objective through focus. However, when the notches were oriented in the 90° configuration, the bilateral symmetry between the tangential and sagittal planes was noticed. Figure 24 shows pictures from going through focus with elliptically-shaped beams in orthogonal directions when moving from the tangential to sagittal focus locations. The microscope objective was positioned at roughly the sagittal and tangential focus locations of the telescope objective and and the resulting spots were projected onto the viewing screen.

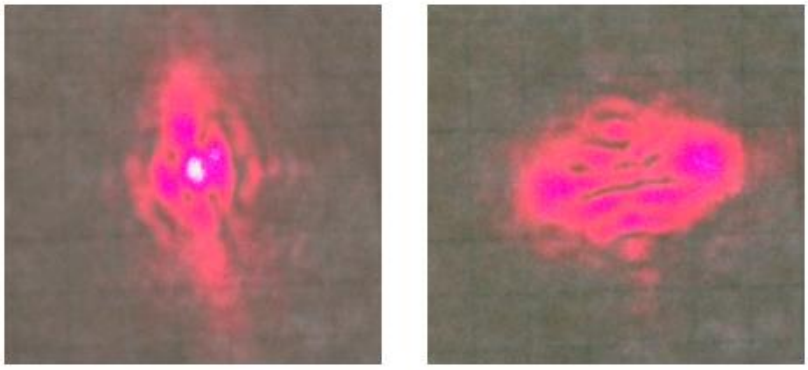

Figure 24. Start Test results for the T21 Objective roughly at sagittal focus (left) and tangential focus(right)

The spots at the best focus position for both lens orientations are shown in Figure 25. With the notches in the nominal orientation, the spot is rotationally symmetric and round in shape. However, with the front lens rotated by 90°, the spot at the medial focus (the location half-way between the sagittal and tangential focus positions) shows a much more astigmatic cross shape and degraded pattern. This provided further evidence that the image quality of the objective can be maximized by visual inspection. It is also important to note the saturation from the camera that is visible in the spot patterns. This shows up as the white areas and is due to the brightness captured by the camera.

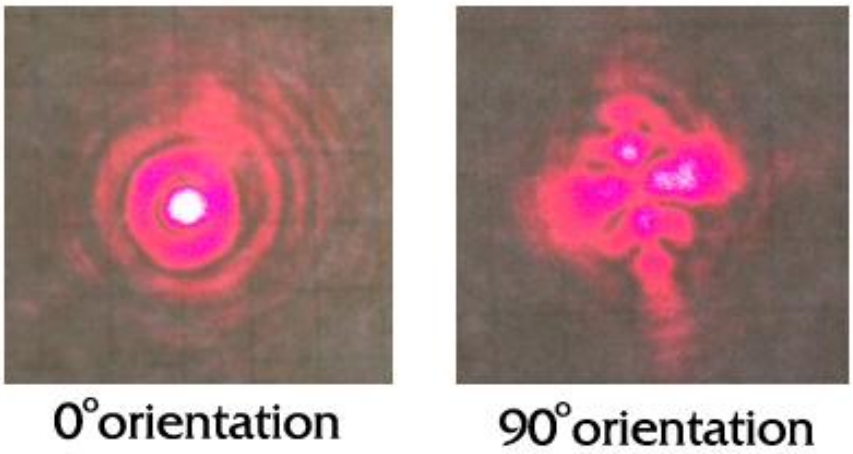

Figure 25. Spots at the medial focus position for both lens orientations

A point spread function was also performed using the computer models from Section 3.2.2 to observe any similarities and is shown in Figure 26. The 0° orientation displays a mostly rotationally symmetric spot while the 90° orientation shows a slight astimatic shape. It appears that the best focus for the computer simulation is near the tangential focus due to the horizontally-shaped spot.

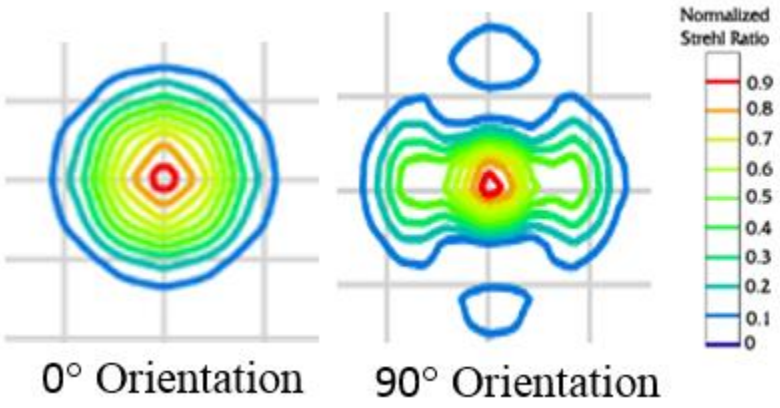

Figure 26. Computer simulated point spread functions for the T21 telescope objective

To further explore the simulation results, the image plane was shifted from the best focus position to roughly locate the best sagittal and tangential focus spots. These images are displayed in Figure 27 and represent the expected trends. Each focus position was obtained by manually moving the the image plane by 50 microns at a time until the optimum location was estimated.

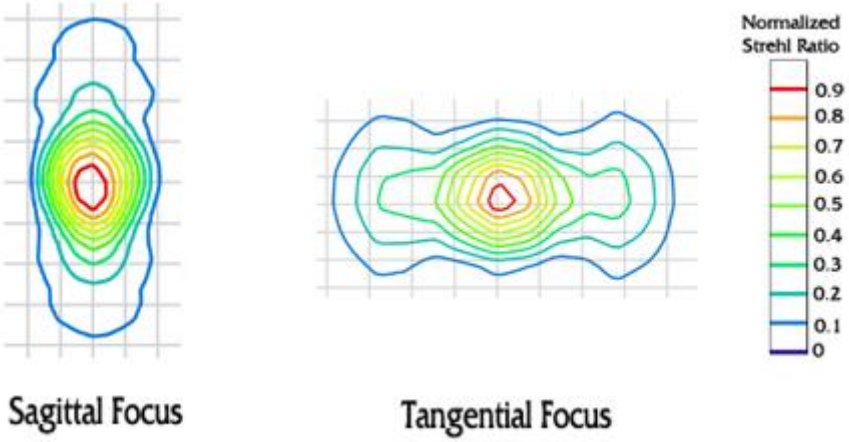

Figure 27. Computer simulated point spread functions for the T21 telescope objective at sagittal and tangential focus

The star test was also performed on the T70 apochromatic triplet objective to try and further quantify the amount of increased astigmatism between the two clocking positions. Because astigmatism dominated this telescope objective and was the main source of wavefront error, it was much easier to observe in the spot patterns and obtain a definitive tangential and sagittal focus position. Figure 28 shows the best focus spot pattern for the T70 objective with the front

lens in the 90° position and the resulting tangential and sagittal focus spots. The cross pattern associated with astigmatism and the two line foci for each focus can be seen.

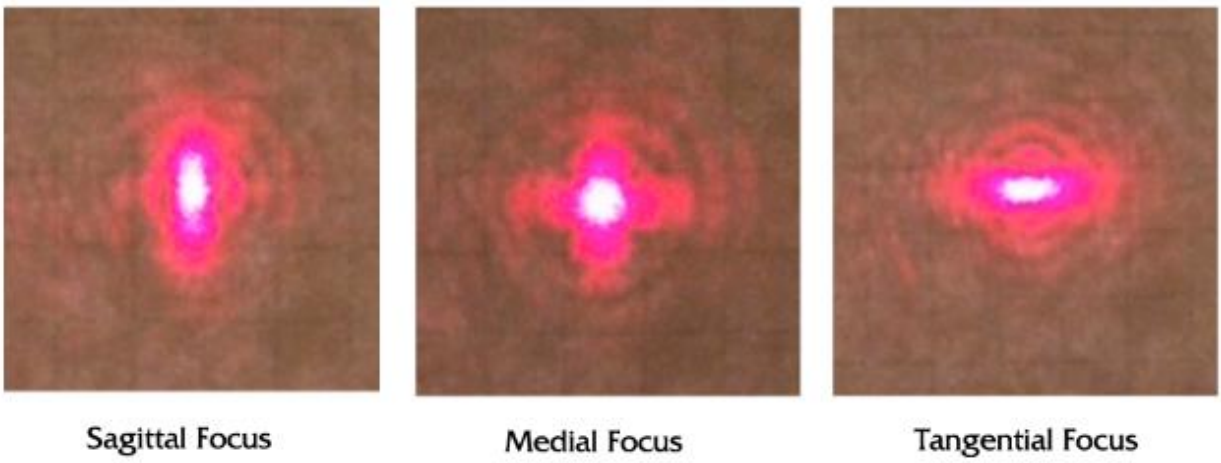

Figure 28. Astigmatic spot pattern with the sagittal and tangential focus position

Although the amount of axial astigmatism was lower in this objective in comparison to the T21 objective, the resulting spot patterns are much more representative of astigmatism. This is due to the fact that astigmatism is mostly responsible for degrading the transmitted wavefront in the T70 objective. Other aberrations such as spherical and coma are very well-corrected for, but astigmatism was still quite prevalent. This is the reason why the star test results show nearly a perfect representation of astigmatism. The T21 objective had a much larger amount of total aberration, and can easily be seen in its star test results. The cross shape is distinguishable, but the addition of coma and spherical aberration increases the complexity of its spot at best focus. Although the magnitude of astigmatism is larger than in the T21, its effects are not as easily observable because of the influence of other aberrations.

The microscope objective that was magnifying the focused spot from the telescope objective was mounted on a micrometer so that it could precisely moved along the optical axis. By recording

the positions at each focus location, the difference between the two was taken, determining the amount of longitudinal aberration. The separation between sagittal and tangential focus was measured to be 527 microns with the f-number of the objective being 12.5. This can then be substituted into the equation:

$$\delta z = -8(f/\#)^2 W_{022} \quad \text{(eq. 4)}$$

to determine the value of the Seidel astigmatism coefficient W_{022}. This resulted in a coefficient value of 0.67 waves for astigmatism in the 90° orientation for the T70 objective. The measured astigmatism value from the transmission test performed in Section 3.1 yielded a value of 0.62 waves, which is very comparable. The slight discrepencies in astigmatism values are due to where each focus location was defined at. Perfect line foci were not produced from the lens, so the most-linear looking pattern was estimated and used.

3.4 Simulating Dispersion

One other hypothesis as to why the objectives were clocked was proposed that it was to minimize dispersion. It was thought that there may have been a significant amount of wedge present in each element that would act as a prism and disperse the light. Thus by orienting each lens properly, the dispersion introduced by from one would cancel with the dispersion introduced by the following lens and chromatic aberrations would be minimized. To test for this, the wedge in the negative element from each objective was measured. A micrometer with precision to the nearest ten-thousandth of an inch was used to measure the edge thickness around the periphery of the lens. By taking the inverse tangent of the edge thickness difference by the clear aperture of the lens, the wedge angle was calculated. The wedge angle for the T21 lens was measured to be 2 arcminutes and the wedge in the T59 and T70 elements were measured to be 1 arcminute.

To see if this amount of wedge introduced a significant amount of chromatic dispersion, a Zemax model was designed. An aberration-free lens was first modeled with an f-number of 10, which is comparable to the T21 objective. A thin prism with a wedge angle of 2 arcminutes was then inserted after the lens and the index was set to BK7 so that dispersion would be introduced. The blur size was then looked at to see how the chromatic effects compared to those from the astigmatism. Figure 29 shows the lateral color obtained from the simulation. These results show that the dispersion from the wedge in the lens creates a 1.4 micron blur size. The lateral color plot also shows the Airy disk for this f-number objective to be 12.2 microns, which the chromatic blur is well under. Compared to astigmatism, the chromatic effects are minimal. The computer model for the T21 objective discussed earlier in Section 3.2.1 results in a blur size of 27 microns. This is much larger than the chromatic blur and over twice the size of the Airy disk. These results provide support that the clocking was not done to minize dispersion from wedge in the lens elements.

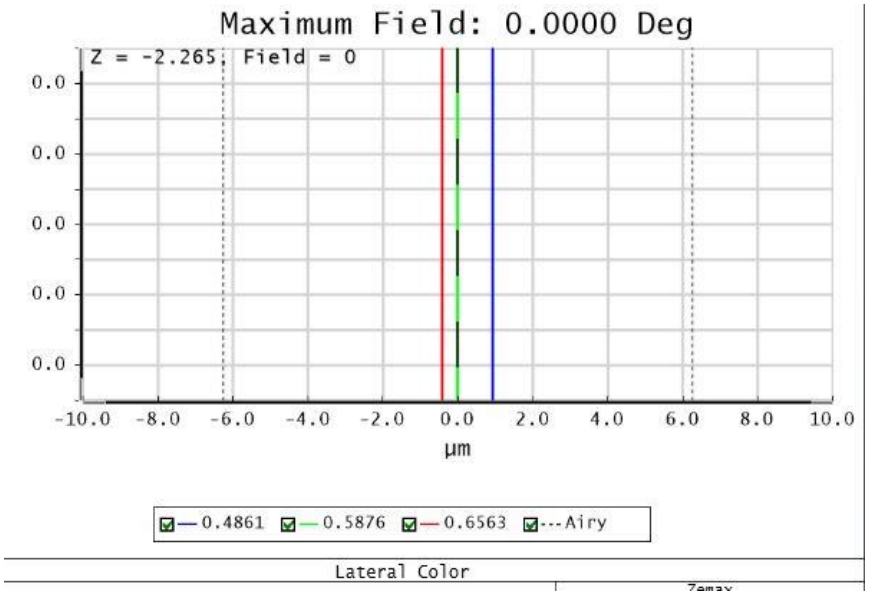

Figure 29. Chromatic blur size from the wedge present in the T21 objective

Chapter 4

Conclusions

These results from the performed tests show strong evidence that there was a purpose behind clocking the telescope objectives. The transmission tests on the lenses provide the best support that astigmatism was maintained by having the correct orientation for each lens with respect to one another. As predicted, rotating one element by 90° to create a crossed configuration doubled the amount of astigmatism. The subtractive effect between surfaces that was occurring with the proper 0° orientation was now reversed to add to the total amount of aberration. The surface tests also provide support to the fact that the rear surfaces of the individual elements did indeed have an astigmatic shape. The difficulties with polishing in the 19th Century was an art form, so the resulting image quality was most susceptible from human error during manufacturing.

The most interesting conclusion arises from Dollond actually testing the objectives. With minimal techniques to test the image quality produced by telescope objectives, Dollond would have been able to properly orient the lenses to reduce aberrations. Using a basic test configuration such as the star test, the optimal orientation of each element in the objectives can be found.

The Museum of Optics of the College of Optical Sciences at the University of Arizona can be viewed online at www.optics.arizona.edu/museum.

REFERENCES

1. J.E. Greivenkamp and D. Steed, "The History of Telescopes ad Binoculars: An Engineering Perspective," in *International Optical Design Conference*, Proc. SPIE-OSA, **8129** 812902-1 (2011).

2. A. Van Helden, "The Invention of the Telescope," Trans of the American Philosophical Society, New Series, **67**(4), 1-67 (1977); reprinted 2008.

3. R. Willach, "The Development of Telescope Optics in the Middle of the Seventeenth Century," Annals of Science, **58**, pp. 381-398 (2001).

4. J. Sasian, "Introduction to Aberrations in Optical Imaging Systems," Cambridge University Press, 2013, pp. 4-9.

5. M. Zghal, "The first steps for learning optics: Ibn Sahl's, Al-Haytham's and Young's works on refraction as typical examples," The Education and Training in Optics and Photonics Conference (International Commission for Optics, 2007.

6. S. Gaukroger, "Descartes: An Intellectual Biography," Oxford Scholarship Online, 1997, pp. 6; reprinted 2003.

7. R. Willach, "The Early History of the Achromatic Telescope Objective," Antique Telescope Society 4th Annual Convention, 29 September, 1996.

8. N. English, " Classical Telescopes: A Guide to Collecting, Restoring, and Using Telescopes of Yesteryear," Springer Science+Business Media, 2013, pp. 2-17.

9. J. Dollond, "An Account on Some Experiments concerning the different Refrangibility of Light," Philosophical Transactions, **50**, pp.733-743 (1757-1758)

10. R. Kingslake, "Who discovered Coddington's equations?" Optics and Photonics News, August 1994, pp. 20-23

11. D. Atchinson and W.N. Charman, "Thomas Young's contributions to geometrical optics," Clinical and Experimental Optometry **94.4**, July 2011, pp. 333-340

12. "Airy's Astigmatism," The Australian Journal of Optometry, 25 October, 1938, pp. 503-507.

13. J. Sasian, “Astigmatism, Field Curvature, and Distortion,” Lens Design OPTI 517, College of Optical Sciences, 2014.

14. R. Willach, “The Development of Lens Grinding and Polishing Techniques in the First Half of the 17th Century,” Bulletin of the Scientific Instrument Society, **68**, pp.10-15 (2001).

15. S. Dupré, “Schyrl de Rheita,” Biographical Encyclopedia of Astronomers, 2007, pp. 966

16. P. Dollond, “An Account of an Improvement made by Mr. Peter Dollond in his New Telescopes,” Philosophical Transactions, **55,** pp. 54-56 (1765)

17. D. Malacara, “Optical Shop Testing,” John Wiley and Sons, Inc; pp. 397-423 1992

APPENDIX

Using the WYKO 6000 – Fizeau Interferometer

Surface Test

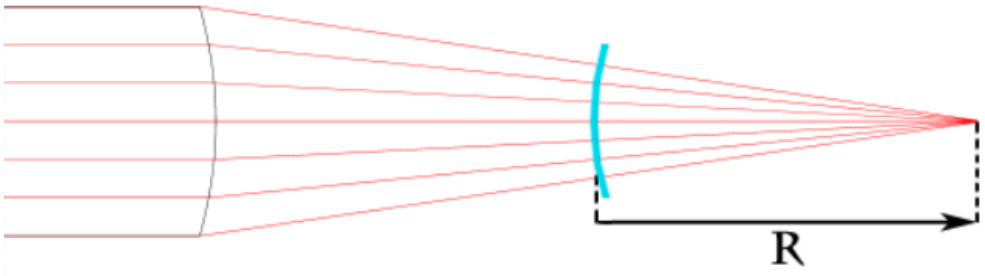

Setup for Testing a Convex Surface

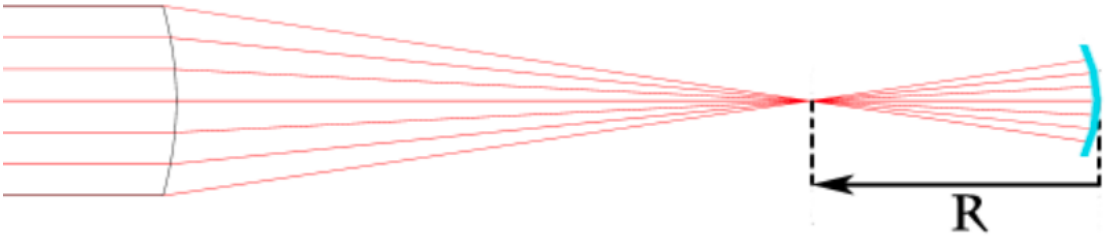

Setup for Testing a Concave Surface

Setting up the Interferometer

- Secure transmission sphere into the interferometer aperture
- Turn the TV on
- Flip the switch on the controller to *Align*
- While in *Align* mode, use the thumbscrews on the interferometer aperture to align the beams on-top of each other

Aligning the Test Surface

- Place the test optic in the mount
- Move the axial position of the test optic along the rail such that the retro-reflected beams come to focus
- Roughly align the surface such that the retro-reflected beams on top of each other as seen on the TV
    - May have to increase the *Intensity* of the beam depending on the test surface
- Further fine tune the alignment using the tip/tilt adjustments on the optic mount

Testing the Test Surface

- Flip the switch on the controller to *Test*
- Fringes should now be visible and some trefoil may be seen because of the supports holding the optic in place
- Further adjust the axial position of the lens and tip/tilt of the optic mount to reach the null fringe
- Adjust the *Zoom* of the camera on the test optic so that it fills the entire screen of the TV
- Adjust the *Focus* of the camera to reduce the diffraction effects at the edges of the test surface

Data Collection

- Open the *4Sight* program on the computer
- Confirm that the *MEAS* screen is open (top left of the window)
- Confirm the settings (right side bar) that '*live feed'* is selected
- Perform a single measurement
- On *Surface* tab (bottom), add an *'A-Mask'* (top bar) to properly select and center the region of interest
    - You may have to delete the *'D-Mask'* before trying to apply an *'A-Mask'* if the software will not allow you to reselect and size the data cursor
    - It may be easier to apply the *'A-Mask'* on the *Modulation* tab (bottom)
- Select *Analysis* (top) → analysis options → statistics
    - Adjust the P-V q percent to where you want most of the data to lie between (typically ~98%)
- Select *Processing Options* (bottom right) → term removal
    - Depending on the test performed, you want to remove certain aberrations. Tilts are most commonly removed because those are most often from alignment. Power may also want to be removed if you are doing a surface vs transmission test.
- Select *Z-Sheet* (top right) to obtain the Zernike aberration values.
    - A 35+ term fit type is often sufficient

** Wedge Factor is 1 for single pass and 0.5 for double pass**

Saving and Re-opening Data

- Tools → Preferences → Saving
    - Make sure the file is not being compressed or minimized
- View (or measure) → measurement flow

Transmission Test

Aligning the Test Lens

- Insert and align a planar mirror in the interferometer's mount (with an ND filter between the interferometer aperture and mirror)
- In a separate mount system, insert the lens inside the assembly and roughly center it
- Move the mirror to roughly cats-eye
- Adjust tip/tilt of the lens to center the small circular fringes on top of each other
- Remove the planar mirror and insert the ball bearing in its place
- Adjust the x and y translations for the ball bearing to center the fringes
- Move the ball bearing towards focus and fine tune the bearing's position to keep the fringes centered

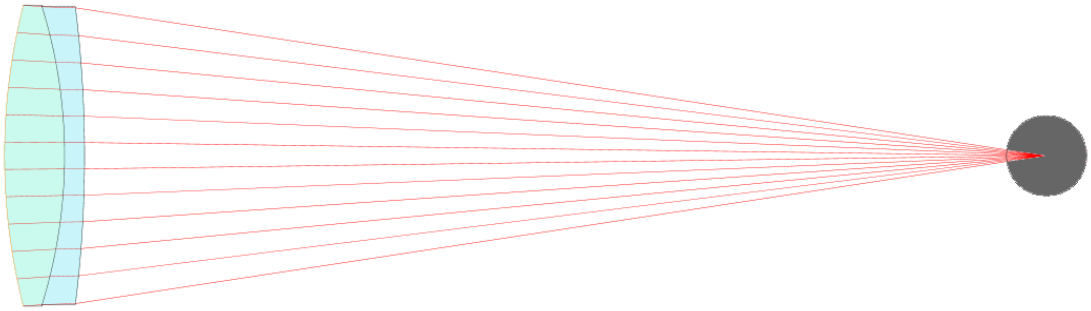

Setup for Transmission Test